




Statistical Perspective on the Petrological Utility of Polyphase Groundmass Compositions Inferred via Defocused Beam Electron Probe Microanalysis

Daniel A. **Coulthard** Jr (1)* , Yoshiyuki **Iizuka** (2), Georg F. **Zellmer** (3)  and Raimundo **Brahm** (4) 

(1) U.S. Geological Survey, Volcano Science Center, 345 Middlefield Road, Mailstop 910, Menlo Park, California 94025, USA

(2) Institute of Earth Sciences, Academia Sinica, No. 128 Sec. 2, Academia Road, Nangang, Taipei 11529, Taiwan

(3) Volcanic Risk Solutions, Massey University, Private Bag 11 222, Palmerston North 4414, New Zealand

(4) School of Geography, Environment and Earth Sciences, Victoria University of Wellington, PO Box 600, Wellington 6140, New Zealand

*Corresponding author. e-mail: dcoulthard@usgs.gov

Polyphase groundmasses (micro-scale minerals with or without glass) are generated from silicate liquids during the cooling of natural lavas often alongside larger minerals formed long before eruption. Many researchers have posited that compositions gleaned from the analysis of groundmasses closely approximate the compositions of the melts they were derived from, and these have been used frequently to model pre-eruptive magma conditions. However, it is difficult to confidently identify and sample these groundmasses once they are formed. Using a sample of lava that exhibits a wide degree of textural variation (ranging from holocrystalline to hypohyaline) we show that compositions of groundmasses sampled using defocused electron beams are significantly different from glass compositions in terms of mean composition and covariance. Despite this, several groundmass compositions qualify as ‘in equilibrium’ with matrix/rim olivine. When processed using available thermometers, however, modelled equilibrium temperatures are significantly higher than those produced using glass data, on average. Because of this, we prescribe caution in using polyphase groundmass data generated using defocused beam analysis even as a rudimentary approach.

Keywords: microanalysis, glass, groundmass, electron microprobe, hygrometry, thermometry, olivine.

Received 26 Apr 23 – Accepted 02 Feb 24

The application of quantitative petrological methods such as mineral-melt thermobarometry requires high-quality compositional data on materials assumed to be in chemical equilibrium with one another. In practice, petrologists often encounter non-ideal sample materials when attempting to quantitatively express the origin(s) of igneous rocks with such methods. Ideally, when interrogating volcanic rocks for information on magma storage, they will be made up of equant and homogeneous crystalline phases set in a homogeneous glass representing a closed system. In many cases open system and kinetic processes have affected natural materials to alter them from their ideal condition, for example through syn/post-eruptive crystallisation. To summarise the problem, the formation of a groundmass during the cooling of natural lavas makes it difficult for petrologists

to confidently quantify the petrogenetic condition(s) that formed the lava under scrutiny using compositional datasets. How many compositions be gleaned from such sample materials to accurately express petrogenesis?

One method may be to mechanically separate matrix fragments for bulk analysis via XRF or ICP-AES. Throughout this text, matrix is used as an umbrella term for glass and/or groundmass and is applied to both macro scale (e.g., hand specimen to mm) and micro scale observations (using either a petrographic microscope or SEM). This method takes an exorbitant amount of time with several processing steps (i.e., separation, weighing, ignition, fusion and other intermediate control measures, such as X-ray diffraction analysis). Importantly, it requires painstaking effort to ensure that

phases non-representative of the melt sub-system be excluded during separation (namely large crystals). It also assumes the absence of foreign materials at the micro-scale (xenocrysts or micro-xenoliths). The inclusion of such material could potentially bias compositional data gathered using bulk methods towards the composition of the contaminant. Instead, the petrologist may be tempted to use a microanalytical approach. EPMA offers efficiency, accessibility and convenience. Sample preparation is limited to selection, mounting, grinding and polishing, and most instruments also include an on-board electron microscope for phase identification and imaging.

Again, two methods are immediately available when using this microanalytical approach. One method involves integrating signal intensities over an area of interest using an electron microprobe equipped with a wavelength dispersive spectrometer (WDS) to produce quantitative concentration maps with pixel values representing the mass fraction of a given element at a given spot on a given image (Barkman *et al.* 2013, Donovan *et al.* 2021). Such maps are analytically expensive, often requiring multiple hours for a given suite of elements for a single sample area. They also require additional post-processing, which enables the calculation of a melt composition through modelling (e.g., mass-balance). The analysis of a polyphase groundmass may also be accomplished using the same approach used to analyse natural glass. That is, with a defocused electron beam.

Defocused beam analysis (DBA) is commonly applied to natural glasses to mitigate the migration of Na (plus K and volatile elements) out of the analysis volume during analysis with a WDS. Frequently, geologists have utilised DBA to analyse sample groundmasses and create placeholder compositions that they claim are representative of the residual melt prior to alteration by syn/post-eruptive crystallisation (e.g., Kimura *et al.* 2005, Noguchi *et al.* 2008, Zellmer *et al.* 2014, Geiger *et al.* 2016, Saito *et al.* 2018). However, the microanalytical community warns against such routines (Barkman *et al.* 2013, Llovet *et al.* 2021). An underlying assumption of quantitative EPMA is that the analysis volume constitutes a homogeneous domain at the micron-scale. This assumption enables the correction of signal intensity using a given matrix correction routine (e.g., the ZAF procedure, Bence and Albee 1968). The assumption is violated when a polyphase material is analysed, and error increases. This is mainly because of averaging correction factors (Llovet *et al.* 2021) and probably also as a function of the size (volume) of the inhomogeneous materials included. Finally, it is important to note that beam diameters over 20 μm are known to generate poor analyses due to geometry.

X-rays emitted far from the beam centre will be defocused to the WDS.

Here we present geochemical data gathered from a New Zealand basalt. These data were gathered on materials representing the residual melt left after eruption of the lava. Locally, glass is preserved alongside equant microcrystalline phases. Elsewhere, pervasive microlite growth has formed a groundmass phase with little glass remaining. Datasets representing these texturally distinct materials are compared with respect to mean composition and sample covariance, and hypothesis testing conducted using these data will determine our confidence in the use of DBA to replicate glass compositions by analysing groundmass. Each dataset is also investigated independently using multivariate statistical methods to further contextualise the results of the hypothesis tests.

Experiment details

Sample description and preparation

For the present study, a sample of basalt originating from Rangitoto Island, New Zealand (Figure 1a), was taken from the rock archive at Massey University, New Zealand. The rock was sourced from a slab flow emplaced along the southern edge of the island (-36.808747, 174.860735, WGS 84). These flows (e.g., Figure 1b) are c. 500 years old (Needham *et al.* 2011) and were erupted during the second phase of magmatism to form the island.

A hammer was used to expose fresh rock surfaces for further processing. Visibly fresh fragments, which were observed to contain abundant olivine macrocrysts (Figure 1c) were either sawed and ground flat for thin sectioning, mounted in 1-inch rounds of epoxy resin as whole rock mounts, or further crushed for mineral and matrix separation. In all cases, fresh rock fragments were ultrasonically treated in de-ionised water to remove debris and dried overnight at 45 °C. From the crushed material, twenty-four olivine macrocrysts and six visually glassy matrix fragments were handpicked to make an additional grain mount. Coarse grinding to polishing used a series of loose SiC grits, microdiamond suspensions and an alumina suspension polishing compound.

Two sample splits were picked for whole rock analysis from the same batch of crushed material. Under the scrutiny of a stereomicroscope, approximately 2 g of rock fragments were gathered indiscriminately and powdered using a

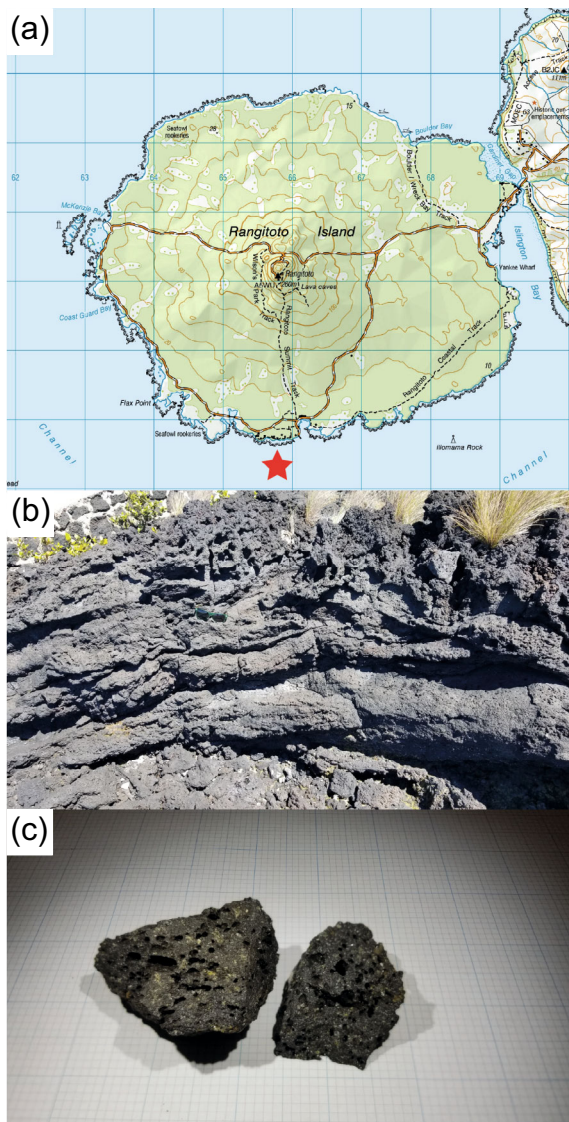


Figure 1. (a) Topographic map of Rangitoto Island adapted from Land Information New Zealand NZ Topo50 Map (available under Creative Commons Attribution 4.0 International – <https://data.linz.govt.nz/license/attribution-4-0-international/>). The site photographed (b) was along the coastline near the red star (where buildings are indicated). (b) Partially eroded flow characteristic of the lavas on this coastline. (c) Fresh surface of the sample material used in this study exhibiting olivine macrocrysts, vesicles and smaller plagioclase meso- and microcrysts. The smallest squares visible on the grid paper in (c) are 1 mm in diameter.

tungsten-carbide ring mill. This split is referred to as bulk rock. The second split was gathered while carefully avoiding olivine macrocryst contamination to represent the matrix of the rock minus the largest olivine phase. This split

(approximately 1 g) was powdered by hand using a quartz mortar and pestle, and it is referred to as matrix.

Prior to ignition for XRF spectrometry, the bulk rock and matrix powders were stored at 110 °C for 2 h, weighed into alumina crucibles at room temperature, placed into an atmospheric muffle furnace, and ignited at 900 °C for 5 h. Once removed from the furnace, we re-weighed the crucibles after cooling for precisely 10 min to measure loss on ignition (LOI). Ignited sample powders were then mixed with a Li-metaborate:Li-tetraborate (12:22) flux in a 1:10 ratio (approximately 0.8 g sample to 8.0 g flux). Fusion and casting utilised an XRFuse2 electronic fusion apparatus to produce uniformly thick glass discs for analysis.

Analytical methods and data quality assessment

Whole rock major element composition was quantified using a 1 kW Bruker Tiger S8 Series II WD-XRF spectrometer at The School of Agriculture and Environment, Massey University, New Zealand. Interference-corrected signal intensities were converted to element oxide mass fractions using calibration curves consisting of natural reference materials. The (long-term) intermediate measurement precision of the instrument was assessed using the basaltic Oreas 24c and granodioritic Oreas 24b reference materials (RMs). Precision (1s) was typically ± 0.5 – 1.0% for major element oxides and better than $\pm 3\%$ relative for minor element oxides, except for P_2O_5 (± 5 – 10%).

Chemical compositions for glass, minerals and ground-mass phases were determined using a Schottky-type JEOL field emission (FE) JXA-8500F EPMA equipped with five WD spectrometers at the Institute of Earth Sciences, Academia Sinica, Taiwan. Back-scattered electron images (BEIs) were taken at this stage using the on-board SEM. Quantitative WD spectrometry was operated at an acceleration voltage of 12 kV with a beam current of 6 nA. A 2 μ m spot diameter was used for mineral analyses, while defocused beam diameters of 5 or 10 μ m were used for glass and groundmass analysis. Use of a 12 kV acceleration voltage, in conjunction with a 6 nA current, has been observed to mitigate beam damage when analysing silicate materials including potentially hydrous glasses and minerals with the FE-EPMA. Prior to gathering the data presented here, when analysed with a 2- μ m beam, glass Na_2O was observed to decrease significantly compared with data gathered using 5 and 10 μ m spot sizes. Since we observed little variation in Na_2O at these latter beam diameters, we initially concluded that these latter settings were suitable for mitigating Na_2O migration.

Table 1.
Calibration material information for EPMA

Element	Crystal	RM name	Composition	Source (JEOL/SPI)
Si	TAP	Wollastonite	CaSiO ₃	JEOL
Ca	PETH	Wollastonite	CaSiO ₃	JEOL
Ti	PET	Rutile	TiO ₂	JEOL
Al	TAP	Corundum	Al ₂ O ₃	JEOL
Cr	PET	Cr Oxide	Cr ₂ O ₃	JEOL
Fe	LiFH	Hematite	Fe ₂ O ₃	SPI
Mn	PET	Mn Oxide	MnO	JEOL
Mg	TAPH	Periclase	MgO	JEOL
Ni	LiFH	Ni Oxide	NiO	JEOL
Na	TAPH	Albite	NaAlSi ₃ O ₈	JEOL
K	PETH	Orthoclase	KAlSi ₃ O ₈	SPI

Measured X-ray intensities were corrected using the PRZ (Oxide-ZAF, via the on-board JEOL software) method using a mixed suite of reference materials (RMs) provided by both JEOL and SPI (Structure Probe, Inc.) Supplies (Table 1). Peak counting of *K α* lines for each element lasted 10 s, while upper and lower background X-rays were counted for 5 s. RMs analysed as unknowns yielded relative standard deviations (1s) of < 1% for Si, Na and K, and < 0.5% for all other elements. Detection limits (2s) were ~ 600–800 $\mu\text{g g}^{-1}$ for all elements except Si (~ 1000 $\mu\text{g g}^{-1}$).

Results

Sample petrography

Throughout this text, we use the crystal size classification scheme of Zellmer (2021). Briefly, microlites are 1–30 μm in width, microcrysts are greater than 30 μm in width but less than 100 μm in length, mesocrysts are between 100–500 μm in length, and macrocrysts are over 500 μm in length. The most abundant mineral in this sample is plagioclase feldspar, which commonly appears both as matrix microlites and as microcrysts, which are barely visible in hand specimen (Figure 2). Large olivine macrocrysts commonly appear in glomerocrysts alongside clinopyroxene and rare large plagioclase mesocrysts (Figure 2c, d). Olivine microlites and microcrysts are also commonly observed. The matrix is both glassy (Figure 2a) and cryptocrystalline (Figure 2c), the latter of which is probably due to sample thickness, which was kept relatively thick to enable later microanalysis.

BEIs taken to guide EPMA revealed matrix textures that were not visible during analysis with a petrographic microscope (Figure 3). Here, we observed a range of textures: areas with clean glass and euhedral-subhedral

microcrysts (Figure 3a), areas which experienced incipient disequilibrium crystallisation producing glass volumes with compositional gradients (Figure 3b), and areas which experienced pervasive disequilibrium crystallisation, which has completely eliminated glass from all but the finest of interstitial volumes (Figure 3c). In the latter two areas, the most commonly observed crystals were feathery clinopyroxene microlites, which formed larger blades as exhibited in Figure 3c. Where these blades have grown particularly large, skeletal oxides are seen also, whose habit resembles those of spinels observed in komatiites.

For our purposes, the last texture was determined to be unsuitable for our microanalytical method due to the size of the feathery pyroxene microlites and the presence of Fe-Ti oxides. Instead, EPMA focused on the textures observed in Figures 3a, b.

Major element compositions and preliminary data screening

All compositional data used in this study, including major element compositions, are freely available for download alongside BEIs and a description of each sample area through Coulthard Jr. *et al.* (2023). Analyses of whole rock samples show that both bulk rock and matrix separates classify as basalts (Figure 4). Table 2 provides compositions for both samples. Negative LOI values were measured for both separates during sample preparation, which we ascribe to a strong degree of sample oxidation. Thus, we recalculated iron speciation assuming a proportion of 0.2 for Fe₂O₃ (reflecting a system buffered approximately to Ni-NiO, which has been assumed elsewhere for primitive lavas of the Auckland Volcanic Field, Brenna *et al.* 2018) and report this mass fraction as well as FeO.

Glass/groundmass compositions whose element oxide totals deviated significantly from 100% (falling beyond a range of approximately 95–102%, accounting for some volatile element mass fractions) were assumed to result from a deficient analysis, and these were discarded outright. Similarly, analyses of olivine were recalculated based on stoichiometric constraints using twelve O atoms for the calculation. Compositions returning model cation totals deviating significantly from accepted values (greater than ± 0.03) were similarly discarded from consideration. In total, forty-seven analyses of visually microlite-free glass had acceptable analytical totals. DBA of partially crystallised glass produced two additional data populations: one gathered using a 5 μm beam, which produced 174 acceptable groundmass compositions, and one using a 10

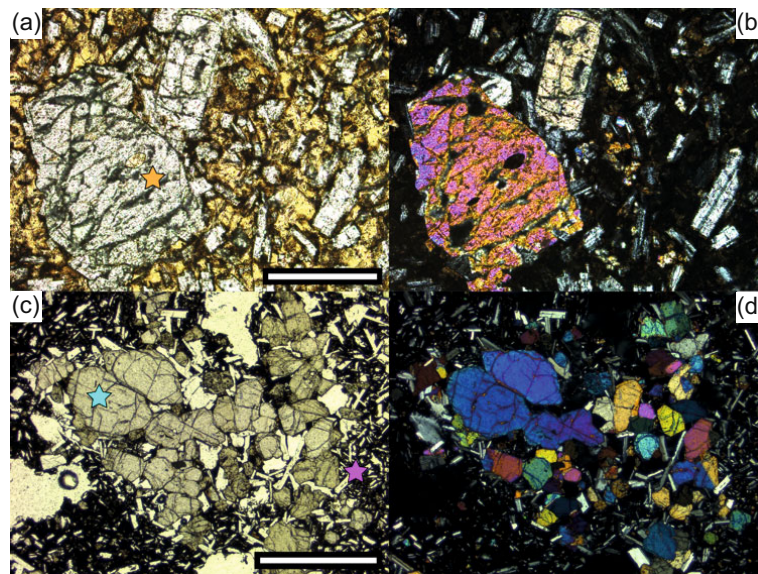


Figure 2. (a) Plane-polarised image of an olivine mesocryst with an exposed melt inclusion (near orange star) set in a glassy matrix containing abundant plagioclase microlites and microcrysts. Scale bar is 350 μm . (b) Cross-polarised image of (a). (c) Glomerocryst containing both olivine macrocrysts (e.g., cyan star), plagioclase mesocrysts and clinopyroxene mesocrysts (e.g., left of purple star, note simple twinning in cross-polarised image). Scale bar is 1.5 mm. (d) Cross-polarised image of (c).

μm wide beam, which produced forty-four compositions. Glass compositions mainly classify as basalt but a few spots trend into the trachybasalt field of the total alkali-silica diagram (Figure 4). On the same plot, we observe that groundmass sampled via both 5 and 10 μm DBA plot as basalt, trachybasalt and basaltic trachyandesite. Olivine core compositions are clearly distinguishable from rim/matrix olivine in terms of forsterite content (Fo#, calculated using moles $\text{Mg}/\text{Mg}+\text{Fe}$, Figure 5) with core composition Fo# ranging between approximately 0.80–0.83, matrix Fo# between approximately 0.69–0.72 and rim Fo# trending slightly higher, from approximately 0.69–0.74. Table 3 contains summary compositional data for the glass, groundmass and olivine data.

Statistical inferences and hypothesis testing

Together, the glass and groundmass compositions represent three datasets to be compared against each other. The two groundmass datasets were grouped based on whether a 5 or 10 μm wide beam was used. Hereafter, these datasets are termed DBA-5 and DBA-10, respectively. Because the following procedure is sensitive to zeros, we elected to reduce the dimensionality of our data and remove select minor element oxides (MnO , Cr_2O_3 and NiO) from consideration. Thus, our input datasets are comprised of

normalised (to 100%) compositions containing the remaining element oxides: SiO_2 , TiO_2 , Al_2O_3 , FeO , MgO , CaO , Na_2O and K_2O .

Each dataset must be determined to be normally distributed in multivariate space prior to any additional hypothesis testing. To this end, we utilised the Anderson-Darling normality test (Anderson and Darling 1952) via the *robCompositions* package (Templ *et al.* 2011) on the R platform (R Core Team 2013). This test implements a Monte Carlo approach and robust estimates of input sample mean and covariance to produce normally distributed synthetic data. Test statistics are then calculated for each of these distributions and compared with the same statistic calculated for the input sample data. The p -value (a value between 0 and 1) returned represents the probability of obtaining a test statistic at least as extreme as the value observed. Low p -values generally indicate that one should reject the null hypothesis (that the input data are normally distributed). Calculated p -values for each dataset are glass = 0.058, DBA-5 < 0.001, and DBA-10 = 0.069. Thus, none of the datasets are likely to be normally distributed.

It is thought that the inclusion of extreme data (outliers) reduces the power of statistical inference especially in small datasets. It is possible that the p -values calculated above led to type I errors (mistaken rejection of a null hypothesis). To

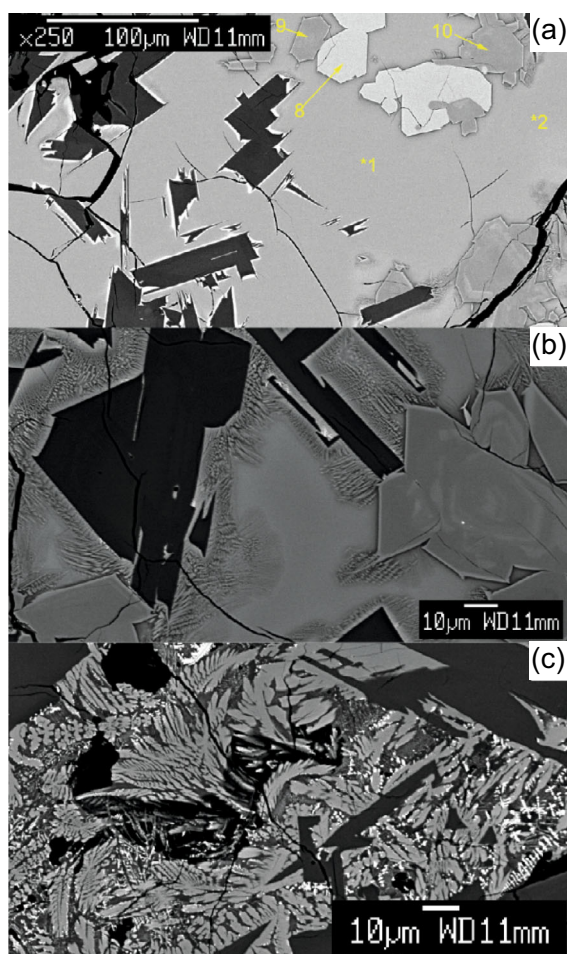


Figure 3. Backscattered electron image gallery. (a) a glass-rich fragment (grain E6, area a) mounted alongside olivine macrocrysts. Analyses marked with * indicate a 5 μm beam was used, while an arrow indicates a 2 μm beam was used. Bright minerals (point 8) are olivine, dark lath-shaped minerals are plagioclase feldspar, and grey minerals (points 9 and 10) are clinopyroxene. (b) A glassy area partially affected by syn/post-eruptive crystallisation. (c) groundmass wholly altered during slow cooling with little to no glass preservation. Note the skeletal Fe-Ti oxides in the interstices between feathery clinopyroxene.

assess for this, we checked each dataset for outliers by first converting each from geochemical data to isometric log ratio (ILR) coordinates (Egozcue *et al.* 2003). The ILR transformation is a necessary step since geochemical data cannot be interrogated using standard statistical approaches due to their closed nature (they are parts of a whole that must sum to an arbitrary constant, see Chayes 1960, Aitchison 1986). Once transformed, the estimate of the sample covariance structure is then used to

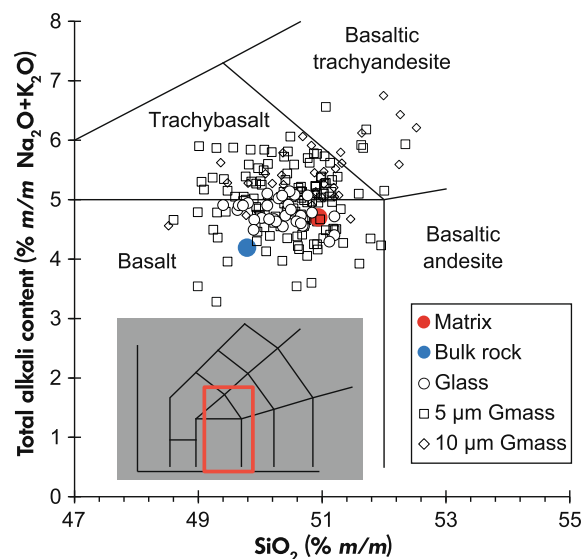


Figure 4. Total alkali-silica diagram. The data shown here have been screened for outlier compositions, as described in the Results section.

Table 2.
Whole rock compositions (% m/m)

	Bulk rock (1 s)	Matrix separate (1 s)
SiO ₂	49.79 (0.34)	50.94 (0.35)
TiO ₂	1.98 (0.06)	2.25 (0.06)
Al ₂ O ₃	14.90 (0.35)	16.67 (0.39)
FeO	8.99 (0.02)	8.39 (0.02)
Fe ₂ O ₃	2.50 (0.02)	2.33 (0.02)
MnO	0.17 (< 0.01)	0.16 (< 0.01)
MgO	9.12 (0.38)	5.64 (0.24)
CaO	9.44 (0.05)	9.95 (0.05)
Na ₂ O	3.44 (0.15)	3.84 (0.17)
K ₂ O	0.75 (0.05)	0.86 (0.06)
P ₂ O ₅	0.31 (0.03)	0.37 (0.03)
LOI	-0.72	-0.58
Total	100.67	100.82
Mg#	0.64	0.55

assess each individual sample for its distance relative to the centre of the data cloud. This distance is referred to as the Mahalanobis distance (MD).

$$MD(x_i) = \left[(x_i - T)' C^{-1} (x_i - T) \right]^{1/2} \text{ for } i = 1, 2, \dots, n \quad (1)$$

from Filzmoser and Hron (2008), where T and C are the location and covariance estimators, respectively. Here, T is the mean and C is the sample covariance matrix. The distribution of squared MDs calculated for each dataset are assumed to approximate a χ^2 distribution with a given

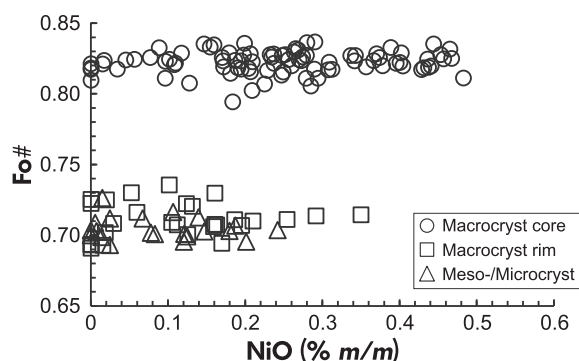


Figure 5. Bivariate chart exhibiting change in olivine composition. High MgO olivine have Fo#s near 0.82, while meso-/microcryst cores and macrocryst rims have lower Fo#s between 0.70–0.77.

number of degrees of freedom. Values above a defined cut-off value, such as the value at the 95% quantile, may be considered as extreme and therefore identified as outliers. This work was performed using the outCoDa function from robCompositions. We assigned a cut-off value at the 95% quantile and used the 'robust' calculation strategy, which automatically converts input geochemical data into pivot coordinates (a special kind of ILR coordinates). Figure 6 identifies the outliers on select bivariate plots.

Within the glass dataset ($n = 47$), sixteen compositions were determined to be outliers. The DBA-5 dataset ($n = 174$) included forty-one outliers, and the DBA-10 dataset ($n = 44$) included twelve. Once these were removed, we reperformed the Anderson-Darling normality tests and produced significantly different p -values: glass = 0.668, DBA-5 = 0.967, and DBA-10 = 0.791. Based on these updated p -values, we fail to reject each null hypothesis. Thus, outlier removal has probably produced normally-distributed data, albeit with different degrees of certainty.

Logically, comparing the means of any two compositions is a way of assessing whether the input groups are similar in multivariate space or not. Similarly, comparing sample covariance matrices assesses for differences in how the individual element oxides within our datasets vary with one another. Following this, four hypotheses may be stated regarding the relationship between any two datasets (after Pawlowsky-Glahn *et al.* 2015):

- (1) The sample means and covariance matrices being compared are insignificantly different from one another;
- (2) The sample means being compared are significantly different from one another, and their covariance matrices are insignificantly different from one another;

Table 3. Representative compositions for matrix datasets and olivine

	Melt compositions			Olivine compositions		
	Glass	DBA-5	DBA-10	Macrocryst core	Mesocryst core	Microcryst/rim
n	47	174	44	38	2	12
SiO ₂	50.35	50.48	50.82	39.58	38.73	37.60
**	(0.46)	(0.70)	(0.88)	(0.45)	(0.35)	(0.40)
TiO ₂	3.33	3.42	3.46	<i>b.d.l.</i>	<i>b.d.l.</i>	<i>b.d.l.</i>
**	(0.17)	(0.21)	(0.27)			
Al ₂ O ₃	12.74	12.74	12.64	<i>b.d.l.</i>	<i>b.d.l.</i>	<i>b.d.l.</i>
**	(0.12)	(0.52)	(0.74)			
FeO _{Total}	12.79	12.91	12.52	16.43	21.48	26.49
**	(0.42)	(1.48)	(1.67)	(0.47)	(0.08)	(0.84)
MgO	4.39	4.25	3.95	43.29	39.55	34.93
**	(0.11)	(0.80)	(0.81)	(0.42)	(0.57)	(0.84)
CaO	8.91	9.18	9.13	0.24	0.31	*0.40
**	(0.20)	(1.15)	(1.18)	(0.03)	(0.05)	(0.07)
Na ₂ O	3.57	3.67	4.16	<i>b.d.l.</i>	<i>b.d.l.</i>	<i>b.d.l.</i>
**	(0.23)	(0.55)	(0.42)			
K ₂ O	1.20	1.29	1.28	<i>b.d.l.</i>	<i>b.d.l.</i>	<i>b.d.l.</i>
**	(0.04)	(0.23)	(0.30)			
Total	97.29	97.93	97.96	99.59	100.19	99.12
Mg#	0.38	0.37	0.36	0.82	0.77	0.70

* Secondary fluorescence probably affects this value.

** Lines below values in parenthesis are 1s uncertainties on the above value.

b.d.l. = Below detection limit.

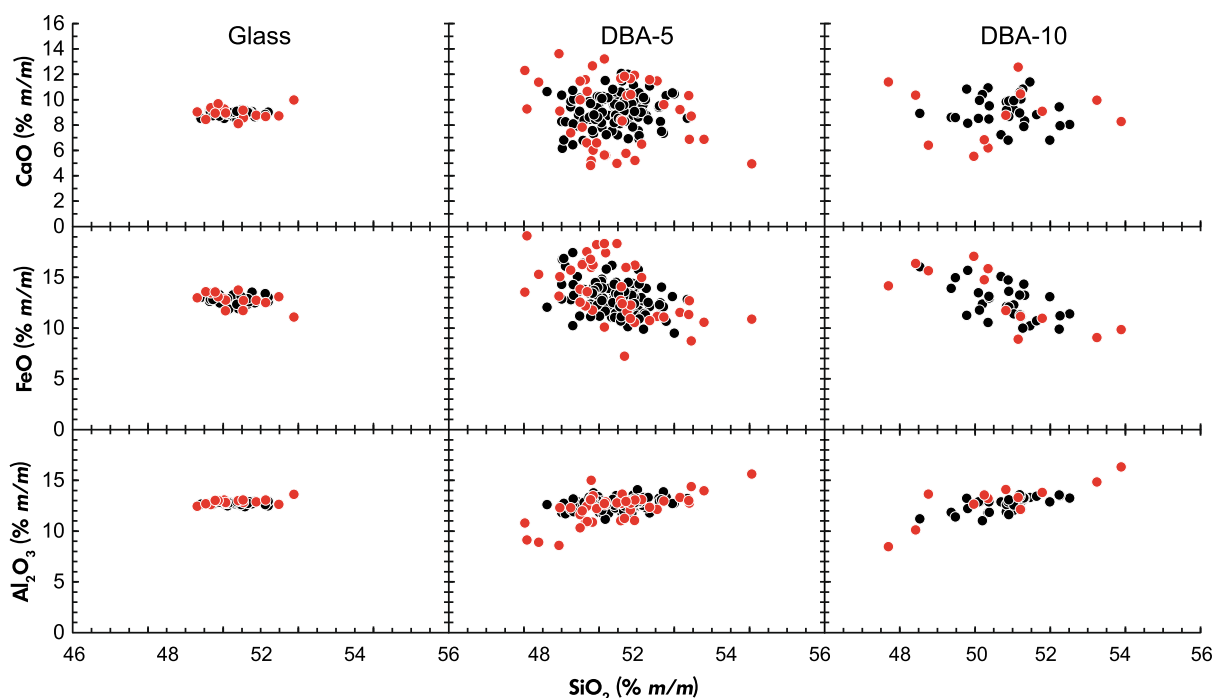


Figure 6. Bivariate plots illustrating select relationships within the glass, DBA-5 and DBA-10 datasets. Multivariate outliers are illustrated as red points.

- (3) The sample means being compared are insignificantly different from one another, and their covariance matrices are significantly different from one another;
- (4) The sample means and covariance matrices being compared are significantly different from one another.

Hypothesis 4 is termed the “general” hypothesis by Pawlowsky-Glahn *et al.* (2015). Each of the other three hypotheses was tested against it as null hypotheses. Intuitively, and following the arguments of many of the authors who have used DBA to approximate melt compositions in the past, one may expect to find similar mean compositions for the glass and either DBA dataset but differences in the way the elements co-vary within each dataset. This is hypothesis 3 above. Using any two pairs of means and covariance matrices, combined/pooled sample estimates were calculated according to Pawlowsky-Glahn *et al.* (2015). All calculations described below were taken from chapter 7.3 of Pawlowsky-Glahn *et al.* (2015), who adapted operations given by (Krzanowski 2000) for compositional data.

These hypothesis tests follow the generalised likelihood ratio test. Considering the maximised likelihood function of any ILR-transformed data under a given null hypothesis, $L_0(X^{ILR})$ and the general hypothesis, $L_g(X^{ILR})$, the test statistic may be approximated.

$$R(X^{ILR}) = L_g(X^{ILR}) / L_0(X^{ILR}) \quad (2)$$

The larger the value of $R(X^{ILR})$, the less likely we are to reject the null hypothesis. Here, the exact distribution of $R(X^{ILR})$ is unknown. Thus, we used Wilks’ asymptotic approximation. Concerning the null hypothesis, the test statistic may be re-written.

$$Q(X^{ILR}) = 2 \ln(R(X^{ILR})) \quad (3)$$

It follows that this test statistic is distributed approximately as $\chi^2(c)$, where c is the number of constraints from the input parameters. The c values used here were calculated using Table 7.1 of Pawlowsky-Glahn *et al.* (2015), and the test statistics calculated here were compared against critical values taken from the upper-tail of a non-centred χ^2 distribution at 95% confidence.

Based on this testing procedure, we rejected each null hypothesis in favour of the general hypothesis when comparing each pair of datasets (summary statistics are provided in Table 4). Thus, we can say with 95% confidence that the sample means and covariance matrices calculated for each dataset (glass, DBA-5 and DBA-10) may be treated as unique and that by extension neither dataset produced

Table 4.
Test statistics for glass-groundmass data comparisons

Null Hypothesis	Parameters for χ^2 distribution		Test statistics*	
	Degrees of freedom	Critical value	DBA-5	DBA-10
Same Mean and Covariance	35	22	362	419
Diff. Mean, Same Covariance	28	17	334	327
Same Mean, Diff. Covariance	7	2	70	81

* To be compared with the Critical value.
italicised = reject Null Hypothesis.

using DBA can be said to approximate the glass data structure.

Principal component analysis

It is not obvious, based on univariate observations (e.g., Figure 6), which geochemical features distinguish the glass data from the DBA-5 and DBA-10 datasets besides minute (and probably spurious) differences in covariation. Principal component analysis (PCA) offers a practical and efficient method of reducing the dimensionality of our datasets such that the internal covariation is illustrated on compositional biplots. Normalised compositions were transformed into centred log ratio (CLR) coordinates (Aitchison 1986) prior to PCA. There are advantages and disadvantages to either transformation, but for our purposes we selected the CLR transformation since it is easier to contextualise the results of PCA in terms of the original input variables (i.e., in terms of individual element oxide variation and covariations). The CLR transformation was performed using the compositions package (van den Boogaart *et al.* 2008), and PCA data are illustrated using the Factoextra (Kassambara and Mundt 2020) and FactoMineR (Lê *et al.* 2008) packages via R.

Figure 7 illustrates how variance is distributed between the PCs for each dataset and is a gross illustration of the

quality of our PCA procedure. The goal is to compress as much variance in as few PCs as possible. These scree plots show that PCs 1–4 explain 86.7% of the variance in the glass dataset. Meanwhile, the same PCs explain 89.2 and 96.9% of the variance in the DBA-5 and DBA-10 datasets, respectively. Thus, most of the information under scrutiny has been compressed into four dimensions.

Compositional biplots (Figure 8) show which elements are represented the most by which PCs as well as which elements correlate with one another in the context of any two plotted PCs. Warm coloured eigenvectors indicate good representation, while cooler colours represent poorer representation. If two eigenvectors are sub-parallel, then this indicates positive correlation between those two variables. If they are opposite one another, then anticorrelation is indicated, and if they are set at a right angle to one another, then non-correlation may be inferred.

Regarding PCs 1 and 2, which contain most of the variance in any dataset, the glass biplot (Figure 8a) illustrates strong anticorrelation between Na and K, anticorrelation between Ca and Fe + Ti (the latter two are weakly represented by these PCs), non-correlation between Na and Ca, Ca and K, and weak correlation between Ca, Al and Si, and between Fe and Ti. Variation of Mg, Fe and Ti are much better represented by PCs 3 and 4 (Figure 8b), with these three elements non-correlating with one another. The biplots

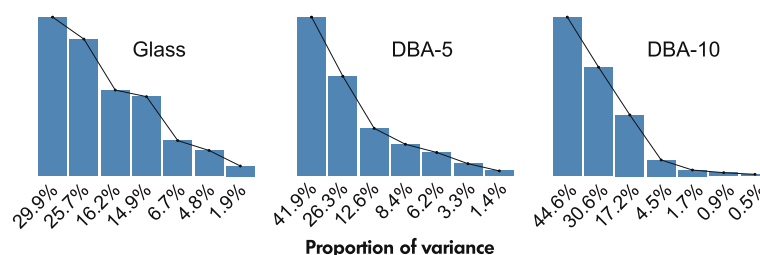


Figure 7. Scree plot detailing the distribution of variance between principal components 1–7 for the glass, DBA-5 and DBA-10 datasets.

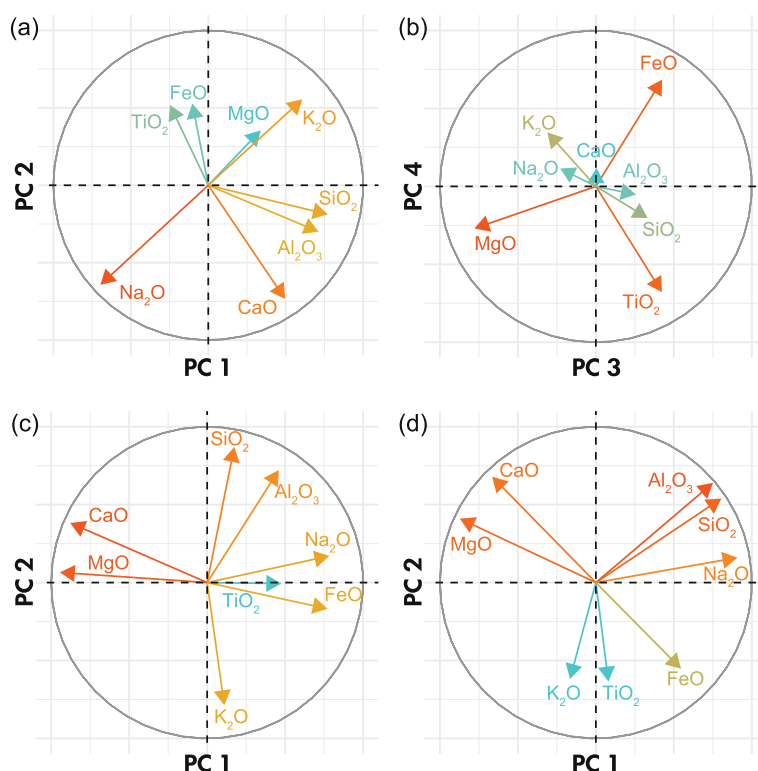


Figure 8. Compositional biplots detailing how variance is distributed for certain elements among certain principal components. For the glass dataset, since a significant portion of variance is distributed between the first four principal components, two biplots (a and b) are included. For the other two datasets, single biplots are included, which explain a majority of the variance. (c) Biplot for DBA-5, and (d) is the biplot for DBA-10. The colours represent how well the variance contributing to the principal components is represented by the elements under scrutiny with warmer colours denoting better representation. For example, see the difference in colour for MgO, FeO and TiO₂ between plots (a) and (b). These element oxides are better represented in by principal components 3 and 4 in (b), as the warmer colours represent this.

for DBA-5 and DBA-10 (Figure 8c, d) provide similar information. In particular, the elements best represented by PCs 1 and 2 on these biplots are Mg, Ca, Al and Si, with Na following. Broadly, Mg and Ca correlate within both datasets as do Al, Si and Na (more so in the DBA-10 dataset). Variation in K, Ti and Fe are poorly represented by these PCs, which together explain nearly 70% of the variance in each dataset.

Discussion

Differences between the glass and DBA datasets

Succinctly, our analysis has shown that DBA of a polyphase groundmass derived from a melt of a given composition probably does not reproduce the composition of glass quenched from that same melt based on the

hypothesis tests summarised in Table 4. This indicates that a significant difference in terms of both mean and covariance distinguish these datasets from one another. Both DBA datasets are highly scattered in compositional space compared with the glass data (Figures 4 and 6). Thus, the precision of DBA, as investigated here using the same or similar analytical conditions as glass analysis, is much worse for any given element oxide when analysing a polyphase groundmass. Furthermore, differences in how individual element oxides correlate with one another (Figure 8) are maximised when considering the glass and DBA datasets separately. Within the glass dataset, correlation between Ca, Al and Si may be attributed to plagioclase fractionation. Since there is little to no correlation between Mg and Ca, there is probably little effect from clinopyroxene crystallisation on the glass dataset. This contrasts with correlation observed within the DBA datasets. Here, Mg and Ca are strongly correlated, which indicates that clinopyroxene fractionation probably sets these data apart. This is consistent with the

observation that the primary phase grown during cooling is feathery pyroxene (Figure 3b). The influence of plagioclase fractionation persists here as well with Na replacing Ca on the biplot (Figure 8c, d).

Based on these observations, we posit that the magma erupted during the formation of Rangitoto Island was actively growing plagioclase feldspar during ascent and eruption but that clinopyroxene growth was limited. Clinopyroxene growth initiated under a depressed thermal gradient and led to the modification of the interstitial melt to form a polyphase groundmass characterised by the presence of feathery pyroxene. This late stage of growth caused fine-scale heterogeneity in the local melt composition, which is evidenced by the appearance of mass fraction gradients in glass (Figure 3b). Fine scale glass heterogeneity, when sampled with the 5 and 10 μm electron beams, probably produced data that form a mixing array in multi-dimensional space.

If our hypothesis testing were conducted using a lower confidence interval (e.g., at 67% confidence instead of 95% confidence), then perhaps our testing would indicate similar means between the glass and DBA dataset(s). This is significant because we have by no means exhausted our analytical capabilities in testing DBA. It could be the case that, with refinement to the analytical conditions, DBA could be better constructed to accurately replicate glass compositions. What we show here is that they cannot be replicated using a similar analytical approach to routine glass analysis.

Regarding covariance, we see no reason to treat these datasets as similar in any significant way. This is bolstered by our PCA, which has shown that there are significant differences in the variances and correlations of individual element oxides between the glass and groundmass datasets.

Alternatively, the cause for the differences between the glass and groundmass datasets could be ascribed to error accrual during measurement. Random error is accrued by the application of DBA to a polyphase groundmass. This is an unavoidable consequence of this method. Functionally, what occurs is an analysis of not one but multiple discrete volumes of material simultaneously. Thus, the analytical volume is always heterogeneous. Ideally, separate matrix correction factors must be calculated for each of these discrete volumes, but this cannot occur when X-rays are being collected within a single point. Thus, the calculated correction factors average out, which is the underlying reason for the random error (Llovet *et al.* 2021). Additionally, based on Figure 4, several analyses of the groundmass

produced compositions with lower SiO_2 than the whole rock composition. This is only possible if these analysis volumes were focused primarily on olivine or on Fe-Ti oxides. This reflects human error, as these analyses represent biased compositions that are too different from the melt composition (at any point during differentiation) to be representative. More careful placement of analysis points should refine the DBA datasets. Another source of error could lie in choosing an improper beam size. Smaller beam sizes applied to a matrix with relatively large microlites could produce data with biased compositions like we observe here. Increasing beam size would increase the probability of sampling a representative matrix volume. This would decrease differences in analytical background as well, which produces analyses with different signal intensities for certain elements. These differences point to a potential solution to DBA in beam size. This would necessitate a distinct analytical routine than that used for glass analysis.

On the utility of DBA for petrological modelling

Given glass and groundmass data represent distinct data structures, it would be injudicious to simply treat them as equivalent for the purpose of petrological modelling. Here, we will perform thermometry using both glass and groundmass compositions (along with paired olivine analyses) in the same way any petrologist might in order to investigate and detail differences in the results obtained from a straightforward application of thermometry.

Figure 9 is an olivine-liquid equilibrium diagram that is commonly used to identify potential input data for

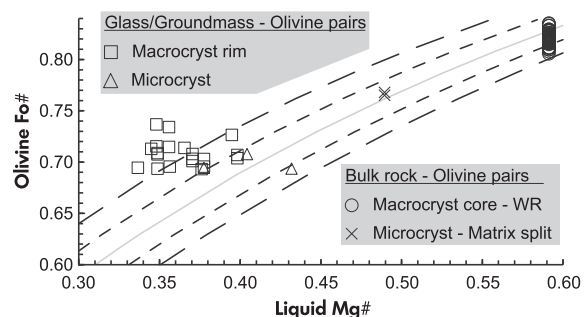


Figure 9. Olivine-liquid equilibrium diagram. The grey line on this chart denotes a distribution coefficient of 0.3, which is commonly taken as the equilibrium distribution coefficient of Mg and Fe between olivine and melt. The finely dashed line represents a 0.03 (1s) envelope around this line, while the coarsely dashed line represents a 0.06 (2s) envelope.

thermometry. The solid line on this diagram represents mineral-melt pairs grown under equilibrium conditions following the observation that Mg and Fe partition between the 2 phases such that $(\text{FeO}/\text{MgO})^{\text{olivine}}/(\text{FeO}/\text{MgO})^{\text{melt}} = 0.30 \pm 0.03$ (1s, Roeder and Emslie 1970). When pairing olivine macrocryst core compositions with the bulk rock composition, we observe that these data plot within this error envelope at the highest end of the diagram. This observation favours an equilibrium condition for the primitive end-member of our geochemical dataset. Zoned olivine microcryst cores pair well with the matrix composition at lower Mg#. The matrix composition obtained using XRF is too high in Mg to pair with olivine microlites or macrocryst rims at the low end of the diagram. Because of this, we must use either glass or groundmass compositions near the microlites/rims themselves. Plotting select pairs shows that there are indeed potential equilibrium pairs within our dataset. Further modelling utilised pairs that plot within 2s of the 0.30 line (eleven pairs in total). Unfortunately, our matrix separation at the macro scale has failed to produce a melt composition in equilibrium with the least forsteritic olivine in our dataset. This is unsurprising considering how small the mineral phases are in this sample.

To keep our modelling simple, since in-depth petrological modelling is beyond the scope of this publication, we assume (1) that the difference between the analytical total of the melt composition used during modelling and a perfect total of 100% is due to the presence of water, (2) that this water is magmatic in origin, and (3) a system pressure of 100 MPa, since the crust at Rangitoto Island is 25 ± 2 km (Stern *et al.* 1987). We utilised equation 22 from Putirka (2008) and these conditions to calculate magmatic temperatures for each olivine-liquid pair that passed our test for equilibrium using Figure 9. These data are plotted in Figure 10 alongside their estimated water mass fractions.

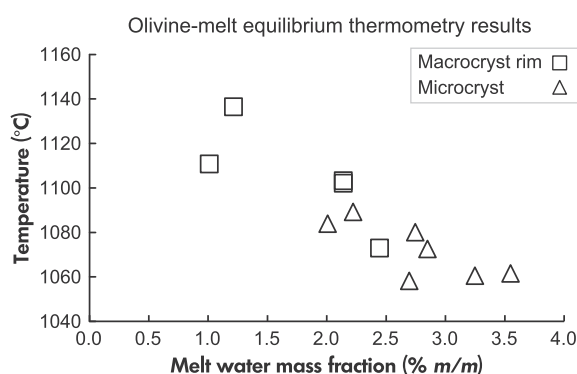


Figure 10. Estimates of temperature and melt water mass fraction from thermometric modelling.

Table 5. Thermometry results

Olivine analysis and point	Glass/groundmass and point(s)	H ₂ O (% m/m)	Temperature (°C)
Rim Analysis; B3c-33	Groundmass; B3c-39:43	1.2	1136
Rim Analysis; B6-1	Groundmass; B6a-13:22	2.4	1073
Microlite; B6c-83	Groundmass; B6c-87-94	2.1	1102
Microlite; B6c-84	Groundmass; B6c-87-94	2.1	1103
Rim Analysis; C6-8	Glass; C6-27:28	2.0	1084
Rim Analysis; C6-8	Groundmass; C6-23:24	1.0	1111
Microlite; D1-10	Glass; D1-11	3.2	1061
Microlite; D2aa-22	Glass; D2aa-11	2.7	1058
Microlite; E2a-3	Glass; E2a-11:12	3.5	1062
Microlite; E2a-4	Glass; E2a-16, 19, 20	2.7	1080
Microlite; E3a-1	Glass; E3a-13:16	2.8	1073
Microlite; E6a-7	Glass; E6a-1:4	2.2	1089

We observe contrast between temperatures estimated using olivine-groundmass pairs and olivine-glass pairs. Olivine-groundmass pairs produced temperature estimates ranging from 1073–1136 °C (five pairs, mean = 1105 ± 23 °C, 1s), while olivine-glass pairs produced estimates ranging from 1058–1089 °C (six pairs, mean = 1072 ± 12 °C, 1s). Thermometry results are summarised in Table 5.

The reason the groundmass compositions produce higher temperature estimates when paired with matrix or rim olivine is because of lower input melt water mass fraction, which is produced by lower average analytical total deficits. The reason groundmass compositions return higher analytical totals is probably because the groundmass analyses were performed on areas with a larger proportion of nominally anhydrous material (pyroxene). Based on the difference between mean temperature estimates (33 °C), we note that a significantly different thermometry result is produced via the substitution of a groundmass composition for a glass composition (at 68% confidence). However, if 2 standard deviations are considered for each population of thermometry data, then we observe overlap in these distributions. Thus, we cannot ascribe a high degree of certainty to the differences observed within the thermometry model output.

Conclusions

We have shown that compositional data generated using routine electron probe methods produce significantly

different data structures when analysing volcanic glass and polyphase groundmasses produced from a melt of the same composition as that of the glass. These data structures are significantly different in terms of both mean composition and covariance, which indicates that they must be approached with caution when utilising them for petrological modelling.

On average, temperature estimates produced using olivine-glass pairs are 33 °C lower than those produced using olivine-groundmass pairs. We show this is primarily due to differences in estimated melt water mass fraction for each set of pairs. This error is significant considering any single equilibrium olivine-melt pair produces a temperature estimate with a standard error of 29 °C.

We consider that the methods we have employed are likely to be widely used at least as a preliminary measure in petrological modelling. If that is the case, then we must prescribe caution when using defocused beam analysis to assess a polyphase groundmass composition (when using the same recipe and beam size as during glass analysis). The results of such a routine cannot be treated as the same as those produced using defocused beam analysis of a uniform and relatively homogeneous material like glass.

Unfortunately, our approach using bulk methods (i.e., separation of whole and matrix rock for X-ray fluorescence analysis) produced results that were biased towards olivine-rich compositions. Our ability to screen mineral phases from the matrix separate proved insufficient, as the matrix composition is not in equilibrium with the least forsteritic olivine. We consider that this is certainly not always going to be the case and that matrix separation for other rock types (e.g., tephra) is likely to see higher rates of success. In the end, we conclude that, without distinct methodological development, defocused beam analysis is an inferior technique to quantitative WDS mapping for quantifying the bulk composition of polyphase groundmass compositions.

Acknowledgements

The authors would like to thank Raimon Tolosana-Delgado and Peter Filzmoser for assistance with the coding behind the hypothesis testing and discussion on statistical methodology. Further thanks go to Tom Sisson, Dawnika Blatter and Dawn Ruth at the USGS for further helpful discussion, and to the four anonymous reviewers who helped shape the final draft. This project was supported by the Royal Society of New Zealand through the Marsden Fund (grant MAU1704 to GFZ) and the U.S. Geological

Survey Volcano Hazards Program. Any use of trade, firm, or product names is for descriptive purposes only and does not imply endorsement by the U.S. Government.

Scientific editing by Paul J. Sylvester.

Data availability statement

All compositional data used in this study, including major element compositions, are freely available for download alongside BEIs and a description of each sample area through Coulthard Jr. *et al.* (2023), <https://doi.org/10.5066/P9PRJSUB>.

References

Aitchison J. (1986)

The statistical analysis of compositional data. Chapman and Hall (London), 416pp.

Anderson T.W. and Darling D.A. (1952)

Asymptotic theory of certain "goodness of fit" criteria based on stochastic processes. *The Annals of Mathematical Statistics*, 23, 193–212.

Barkman J.E., Carpenter P., Zhao J.C. and Donovan J.J. (2013)

Electron microprobe quantitative mapping vs. defocused beam analysis. *Microscopy and Microanalysis*, 19, 848–849.

Bence A.E. and Albee A.L. (1968)

Empirical correction factors for the electron microanalysis of silicates and oxides. *The Journal of Geology*, 76, 382–403.

Brenna M., Cronin S.J., Smith I.E.M., Tollan P.M.E., Scott J.M., Prior D.J., Bamberg K. and Ukstins I.A. (2018)

Olivine xenocryst diffusion reveals rapid monogenetic basaltic magma ascent following complex storage at Pupuke Maar, Auckland Volcanic Field, New Zealand. *Earth and Planetary Science Letters*, 499, 13–22.

Chayes F. (1960)

On correlation between variables of constant sum. *Journal of Geophysical Research*, 65, 4185–4193.

Coulthard Jr. D.A., Iizuka Y., Zellmer G.F. and Brahm R. (2023)

Data support for a statistical perspective on the petrologic utility of polyphase groundmass compositions inferred via defocused beam electron probe microanalysis. U.S. Geological Survey data release. <https://doi.org/10.5066/P9PRJSUB>



references

- Donovan J.J., Allaz J.M., von der Handt A., Seward G.G.E., Neill O., Goemann K., Chouinard J. and Carpenter P.K. (2021)**
Quantitative WDS compositional mapping using the electron microprobe. *American Mineralogist*, 106, 1717–1735.
- Egozcue J.J., Pawlowsky-Glahn V., Mateu-Figueras G. and Barceló-Vidal C. (2003)**
Isometric logratio transformations for compositional data analysis. *Mathematical Geology*, 35, 279–300.
- Filzmoser P. and Hron K. (2008)**
Outlier detection for compositional data using robust methods. *Mathematical Geosciences*, 40, 233–248.
- Geiger H., Mattsson T., Deegan F.M., Troll V.R., Burchardt S., Gudmundsson Ó., Tryggvason A., Krumbholz M. and Harris C. (2016)**
Magma plumbing for the 2014–2015 Holuhraun eruption, Iceland. *Geochemistry, Geophysics, Geosystems*, 17, 2953–2968.
- Kassambara A. and Mundt F. (2020)**
Factoextra: Extract and visualize the results of multivariate data analyses. R package version 1.0.7.
- Kimura M., Weisberg M.K., Lin Y., Suzuki A., Ohtani E. and Okazaki R. (2005)**
Thermal history of the enstatite chondrites from silica polymorphs. *Meteoritics and Planetary Science*, 40, 855–868.
- Krzanowski W. (2000)**
Principles of multivariate analysis. Oxford University Press (Oxford), 586pp.
- Lê S., Josse J. and Husson F. (2008)**
FactoMineR: An R package for multivariate analysis. *Journal of Statistical Software*, 25, 1–18.
- Llovet X., Moy A., Pinard P.T. and Fournelle J.H. (2021)**
Electron probe microanalysis: A review of recent developments and applications in materials science and engineering. *Progress in Materials Science*, 116, 100673.
- Needham A.J., Lindsay J.M., Smith I.E.M., Augustinus P. and Shane P.A. (2011)**
Sequential eruption of alkaline and sub-alkaline magmas from a small monogenetic volcano in the Auckland Volcanic Field, New Zealand. *Journal of Volcanology and Geothermal Research*, 201, 126–142.
- Noguchi S., Toramaru A. and Nakada S. (2008)**
Groundmass crystallization in dacite dykes taken in Unzen Scientific Drilling Project (USDP-4). *Journal of Volcanology and Geothermal Research*, 175, 71–81.
- Pawlowsky-Glahn V., Egozcue J.J. and Tolosana-Delgado R. (2015)**
Modeling and analysis of compositional data. Wiley (Chichester), 272pp.
- Putirka K.D. (2008)**
Thermometers and barometers for volcanic systems. *Reviews in Mineralogy and Geochemistry*, 69, 61–120.
- R Core Team (2013)**
R: A language and environment for statistical computing.
- Roeder P.L. and Emslie R.F. (1970)**
Olivine-liquid equilibrium. *Contributions to Mineralogy and Petrology*, 29, 275–289.
- Saito G., Ishizuka O., Ishizuka Y., Hoshizumi H. and Miyagi I. (2018)**
Petrological characteristics and volatile content of magma of the 1979, 1989, and 2014 eruptions of Nakadake, Aso volcano, Japan. *Earth, Planets and Space*, 70, 197.
- Stem T., Smith E.G.C., Davey F.J. and Muirhead K.J. (1987)**
Crustal and upper mantle structure of the northwestern North Island, New Zealand, from seismic refraction data. *Geophysical Journal International*, 91, 913–936.
- Templ M., Hron K. and Filzmoser P. (2011)**
robCompositions: An R-package for robust statistical analysis of compositional data. *Compositional Data Analysis: Theory and applications*, 341–355.
- Zellmer G.F., Sakamoto N., Iizuka Y., Miyoshi M., Tamura Y., Hsieh H.-H. and Yurimoto H. (2014)**
Crystal uptake into aphyric arc melts: Insights from two-pyroxene pseudo-decompression paths, plagioclase hygrometry, and measurement of hydrogen in olivines from mafic volcanics of SW Japan. In: Gomez-Tuena A., Straub S.M. and Zellmer G.F. (eds), *Orogenic andesites and crustal growth*. Geological Society of London, Special Publication, 385, 161–184.
- Zellmer G.F. (2021)**
Gaining acuity on crystal terminology in volcanic rocks. *Bulletin of Volcanology*, 83, 78.